Highly sensitive fiber refractive index sensor based on side-core holey structure*

Han Ya(韩 雅), Xia Li(夏 历)†, and Liu De-Ming(刘德明)

Next Generation Internet Access National Engineering Laboratory (NGIA), School of Optical and Electronic Information, Huazhong University of Science and Technology (HUST), Wuhan 430074, *China*

(Received 21 November 2013; revised manuscript received 28 March 2014; published online 10 August 2014)

We propose a side-core holey fiber (SCHF)-based surface plasmon resonance (SPR) sensor to achieve high refractive index (RI) sensitivity. The SCHF structure can facilitate analyte filling and enhance the overlapping area of the core mode and surface plasmon polariton (SPP) mode. The coupling properties of the sensor are analyzed by numerical simulation. The maximum sensitivity of 5000 nm/RIU in an RI range of 1.33–1.44, and the average sensitivity of 9295 nm/RIU in an RI range from 1.44 to 1.54 can be obtained.

Keywords: holy fiber, surface plasmon resonance, refractive index, fiber sensor

PACS: 42.81.–i, 42.81.Pa, 71.45.Gm **DOI:** 10.1088/1674-1056/23/10/104219

1. Introduction

The fiber-based plasmonic refractive index (RI) sensors have attracted much attention in the context of biochemical analysis without molecule labeling lately.[1,2] As we know, surface plasmon resonance (SPR) sensor is highly sensitive to the variation in RI of the dielectric adjacent to metal.[3,4] The holey fibers (HFs) can be designed flexibly to achieve some specific functions.[5–7] The HF-based SPR sensors have benefited from the improvements in fiber fabrication and hole-coating technologies. Due to the extremely high sensitivity, small size, capable of being distributed online and closed-form all-in-fiber sensing, more and more researchers dedicated their efforts to the design of HF-SPR sensors.

To realize the fiber-based SPR sensing, one essential condition is to equate the effective refractive index of the waveguide core mode to that of SPP mode, which is the requirement for phase matching. Hassani and Skorobogatiy[8] pointed out that the phase matching and packaging issues of SPR sensor can both be addressed using PCFs. On the basis of Hassani and Skorobogatiy's structure, Yu *et al.*[9] proposed a selectively coated HF-SPR sensor, which has reduced a number of metalized microchannels and improved resonance width and depth. Zhang *et al.*[10] added an analyte channel into the waveguide core region of the structure to improve the sensing parameters of the sensor, and they obtained a better detection limit, larger signal-to-noise ratio (SNR), and higher linearity. Zhou *et al.*[11] combined plasmonic resonance and directional-waveguide coupling to achieve a very large dynamic sensing range.

The common feature of these HF-SPR sensors is the several neighboring metalized channels. They have the following disadvantages: (i) the existence of many metalized channels increases fabrication cost and absorption loss, and deteriorates the SNR, (ii) the closely arranged metalized channels interfere with each other and form many complex mode patterns which have the same SPP mode order, which leads to a wide resonance spectral width during mode coupling of waveguide core mode and SPP mode.

After investigating the dual-core microstructure optical fiber,[12] we add a metal layer in the left core which works as an analyte channel in the SCHF. The design is free of selective analyte-filling. In this paper we try to simplify the structure as far as possible: i) only two channels are considered. One is the optical channel delivering laser and the other is a sensing channel with analyte filled in. ii) the dual-core microstructure is chosen to enlarge the overlapping area of the waveguide core mode and SPP mode. The optimized structure will be demonstrated to have a higher sensitivity. The capability of the SCHF-SPR sensor in RI detection is analyzed by numerical simulation. The rest of this paper is organized as follows. In Section 2, the sensor geometry design and numerical modeling are depicted in detail. Mode analysis is conducted in Section 3 to select the proper guiding mode and target sensing SPP mode. The anti-crossing effect is also presented theoretically. In Section 4, the sensing performance of the SCHF-SPR sensor is studied. In Section 5, the conclusions are given.

2. Sensor geometry design and theoretical modeling

The cross section of the SCHF-SPR sensor for computation is shown in Fig. 1(a). The silica microstructure fiber can be fabricated through a standard stack-and-draw process.[13]

*Project supported by the Major Projects of the National Natural Science Foundation of China (Grant No. 61290315), the National Natural Science Foundation of China (Grant No. 61340057), and the Special Program of the National Modern Service Industrial Development Foundation of China (Grant No. [2012]14).

†Corresponding author. E-mail: xiali@hust.edu.cn

© 2014 Chinese Physical Society and IOP Publishing Ltd

We assume that the background RI of SCHF is 1.45, representing the silica glass. The hole-to-hole pitch is $\Lambda = 2$ μm. The left channel, with a diameter of $d_a = 0.8\Lambda$, is coated by gold with a thick layer of $t = 40$ nm for analyte infiltration. Other holes, with a diameter of $d = 0.5\Lambda$, are air-filled to ensure mode guidance in the right core. The permittivity of gold is defined by the Drude model. RI of analyte n_a ranges from 1.33 to 1.54. The finite element method (FEM) is used for mode analysis. A perfectly matched layers (PML) is added to the outer layer to study the loss property of the proposed sensor. Figure 1(b) shows the mesh profile of the SCHF structure. Only half of the structure needs to be computed due to the symmetry along the x axis. A perfect magnetic conductor (PMC) or perfect electric conductor (PEC) condition is added along the x axis to simulate the x-polarized mode or y-polarized mode, respectively.[14]

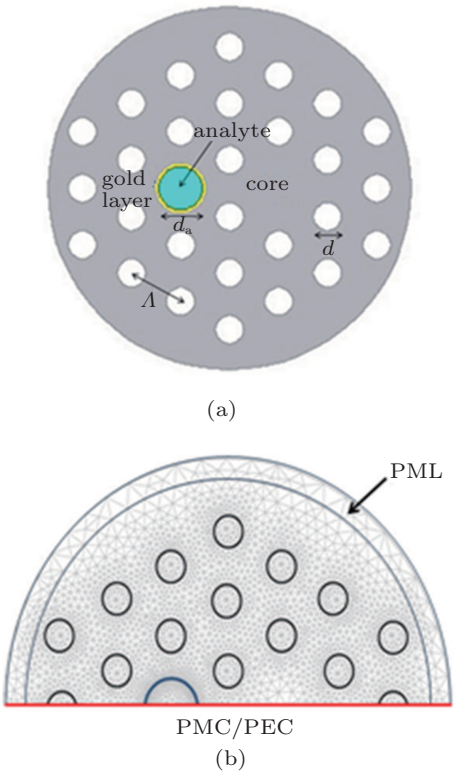


Fig. 1. (color online) (a) Schematic illustration of the SCHF-SPR sensor, and (b) example of FEM mesh and artificial boundary conditions.

3. Mode analysis

3.1. Selection of the SPP mode and guided mode

The index guiding SCHF consists of a waveguide core and an analyte-filling channel. Unlike a conventional dual-core microstructure, the left core of the fiber is omitted and replaced with a cylindrical analyte channel coated with a thin metal layer. Thus the mode coupling mechanism is SPR. In our design, except for the analyte channel in the left core region, the other circular holes are all air holes which ensure light guidance in the solid core. We simulate the effective mode index in a wide wavelength range to find the SPP mode coupling to the fundamental core mode.

As shown in Fig. 2, the x-polarized light in the SCHF structure experiences a stronger resonance coupling than the y-polarized light. The SCHF structure is asymmetric along the y axis, which induces a modal birefringence.[15,16] The original core-guided mode is degenerated into two orthogonally polarized modes: one is parallel to the x axis which is the symmetry axis of the RI distribution, and the other one is perpendicular to it. The symmetry RI distribution along the x axis strengthens the overlapping electrical distribution between the x-polarized fundamental (fundx) mode and SPP (sppx) mode. Electric field of fundx mode more infiltrates into the analyte channel at the phase matching point. Compared with the y-polarized fundamental (fundy) mode, the fundx mode presents a sharp resonance peak, which will facilitate the detection of a resonant-based RI sensor. Thus, the fundx mode is selected as a guided mode in the following work.

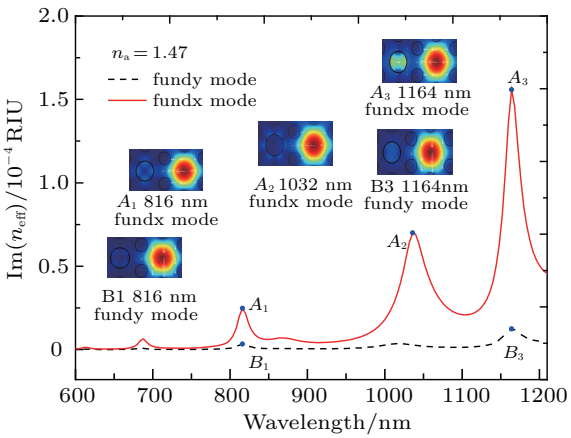


Fig. 2. (color online) Loss curves of fundx mode and fundy mode when $n_a = 1.47$. Insets A_1–B_3 show the electric field distributions for fundamental core mode at the corresponding resonant wavelength.

The dispersion and loss curves of fundx mode and sppx mode are presented in Fig. 3. The analyte RI is 1.47 in Fig. 3(a), neither the fundx mode nor the x-polarized 3rd order SPP (spp_3x) mode is sensitive to the RI change. It should be noted that spp_3x mode is confined to the interface between gold and silica, and the RI of silica is constant in our simulation, thus the resonant peak will not be affected by the RI change of the analyte. The insets show the electric field distributions of the related sppx mode. The 2nd-order sppx (spp_2x) mode and 1st-order sppx (spp_1x) mode match with fundx mode at 724 nm and 890 nm respectively when $n_a = 1.44$, at 816 nm and 1168 nm respectively when $n_a = 1.47$. With an RI change of 0.03, the resonant wavelength shifts of spp_2x mode and spp_1x mode are 88 nm and 278 nm respectively. The spp_1x mode is more sensitive to the RI change of the analyte. Thus the spp_1x mode is the target plasmonic mode for RI sensing in SCHF structure.

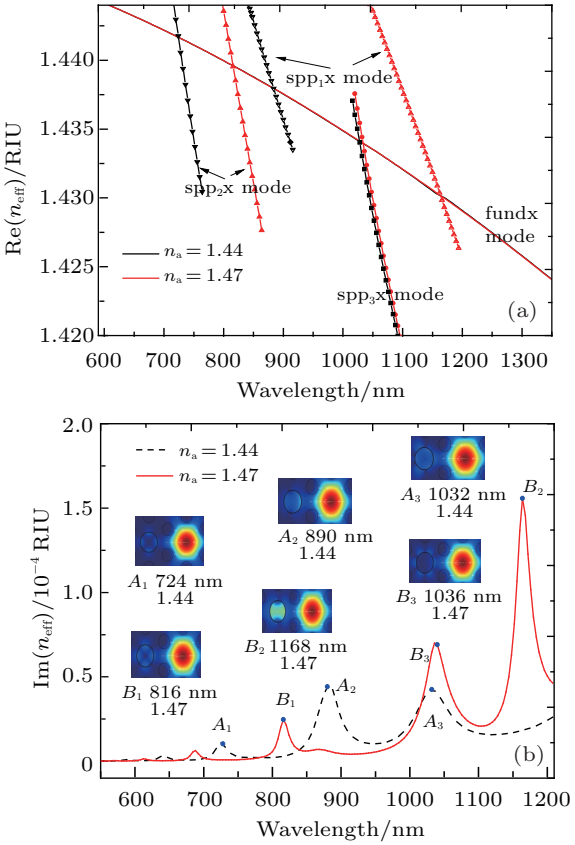


Fig. 3. (color online) Dispersion relations (a) and loss curves (b) of fundx mode and sppx mode when $n_a = 1.44$, 1.47. Insets A_1–B_3 show the electric field distributions for fundamental core mode at the corresponding resonant wavelength.

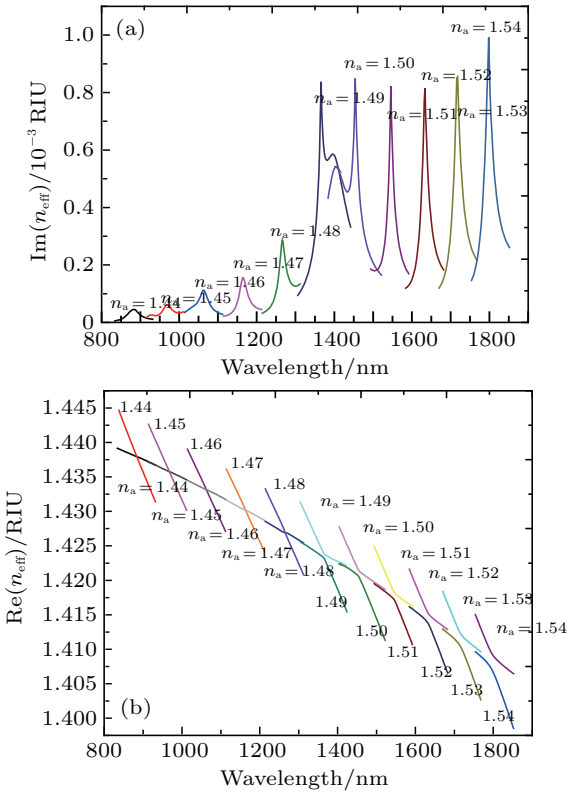


Fig. 4. (color online) (a) Loss curves of RI ranging from 1.44 to 1.54, and (b) dispersion graph of RI ranging from 1.44 to 1.54.

3.2. Anti-crossing effect at large n_a

The resonant curves for n_a changing from 1.44 to 1.54 are depicted in Fig. 4. When $n_a \geq 1.49$, the anti-crossing effect appears. A detailed mode analysis for $n_a = 1.50$ is performed to illustrate the anti-crossing effect.

Figure 5(a) shows that 1) the originally intersecting dispersion curves split into two new modes (the odd supermode and the even supermode); 2) instead of the dip-to-peak loss difference,[17] the loss curves of the two new modes intersect at the anti-crossing point (Fig. 5(b)).

The coupled mode theory[18] can be used to explain the anti-crossing effect of the SCHF sensor. The SCHF is composed of two optical waveguides: solid core PCF waveguide and plasmonic waveguide. The dashed line in Fig. 5(a) depicted the dispersion curve of the stable transfer mode of these two waveguides. The stable transfer mode of the SCHF is different from the mode that propagates independently in the two waveguides. Higher leads to a big coupling coefficient between the fundx mode and spp$_1$x mode, so the coexistence of the two waveguides leads to two supermodes. According to Ref. [18], the propagation constants of the supermode are

$$\beta_{\pm} = \frac{\beta_f + \beta_p}{2} \pm \left[\kappa^2 + \delta^2\right]^{1/2}, \quad \delta = \frac{(\beta_f - \beta_p)}{2}, \qquad (1)$$

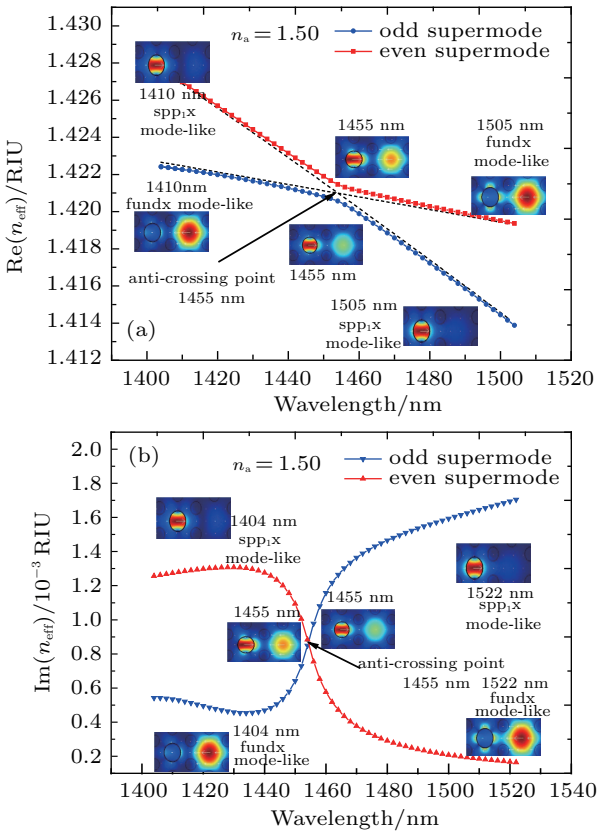


Fig. 5. (color online) (a) Dispersion curves and (b) loss spectra versus wavelength at $n_a = 1.50$. The short dotted line in panel (a) represents the dispersion curves of the spp$_1$x mode and fundx mode which propagate independently. The insets correspond to electric field distributions of the coupled modes at the selected wavelength.

where β_f and β_p are the propagation constants of the solid core PCF and plasmonic waveguide respectively, κ is the coupling coefficient, and δ is the detuning factor. At the wavelength that deviates from the anti-crossing point, the propagation constants of the even supermode and odd supermode are close to those corresponding to the dispersion curve of the relevant isolate waveguide, thus the electric field distribution of the supermode is almost the same as the distribution in the relevant isolate waveguide. When the wavelength is close to the anti-crossing point, the propagation constant of the even supermode is almost equal to that of the odd supermode, with a π phase difference. Figure 6 exhibits the axial pointing vector distributions of the even and odd supermodes at the selected wavelength when $n_a = 1.50$. A qualitative description of the anti-crossing effect can be concluded from Fig. 5. At short wavelength far from the wavelength of anti-crossing point, the mode fields of the even supermode and the odd supermode are confined well in analyte channel and core region respectively. So the electric field distributions of the even supermode and the odd supermode are just like those of the spp_1x mode and fundx mode respectively. As the wavelength increases, the mode field of the even supermode leaks from the analyte channel to core region meanwhile the mode field of the odd supermode leaks from core region to the analyte channel gradually. When the wavelength is close to the wavelength of anti-crossing point, the field intensity of the even supermode and odd supermode are almost the same. At a longer wavelength which deviates from the wavelength of anti-crossing point, almost the whole mode field in core region transfers to the analyte channel for the even supermode. The transition for the odd supermode is just contrary to that for even supermode. Then the electric field distributions of the even supermode and the odd supermode are interchanged into the fundx mode and spp_1x mode, respectively. Figure 5(b) presents the imaginary parts of the two supermodes. It is clearly seen that the imaginary parts of the two supermodes are equal at the wavelength of anti-crossing point.

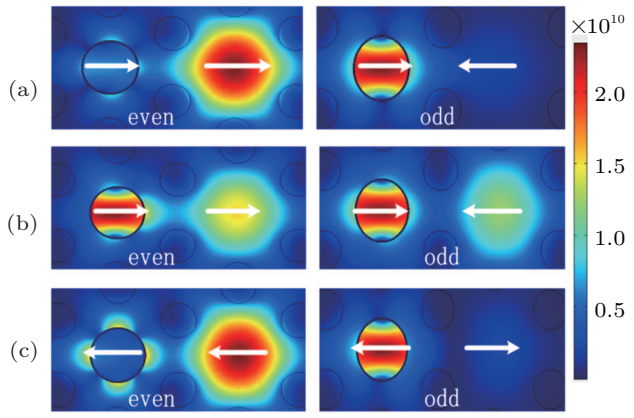


Fig. 6. (color online) Axial pointing vector distributions of the even and odd supermodes at (a) 1400 nm, (b) 1455 nm (the resonant wavelength), and (c) 1500 nm when $n_a = 1.50$.

4. Sensing performance

In this section, the resonant spectra of the core mode are calculated to evaluate the SCHF's sensing performance. The results are shown in Fig. 7.

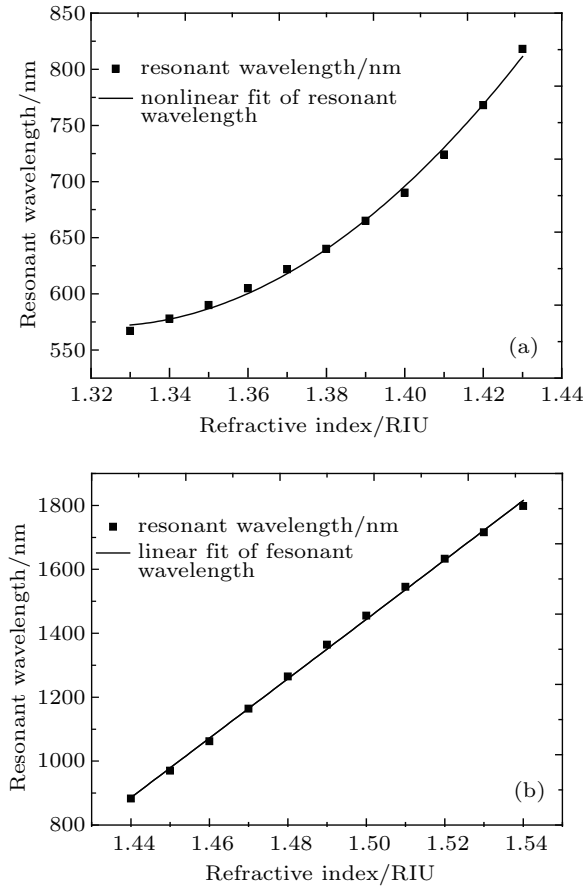


Fig. 7. Response curves of the SCHF-SPR sensor (a) for a dynamic RI range of 1.33–1.43 and (b) for RI range of 1.44–1.54.

The sensitivity for a resonance-based RI sensor is often defined as $S_\lambda(\text{nm/RIU}) = \mathrm{d}\lambda_{peak}/\mathrm{d}n_a$.[20] So the average sensitivity can be obtained from the slope of the linear fitting line. As shown in Fig. 7, the response curve shows a high linearity in a higher RI range from 1.44 to 1.54, while exhibiting a nonlinear character in a lower RI range from 1.33 to 1.43. Thus we divide the RI range of the analyte into two subranges: 1.33–1.44 and 1.44–1.54. The fitting equations and adjusted R-square (*ARS*) values for the dynamic RI are

$$\lambda_l(\text{nm}) = 36937.7040 - 54996.5035n_a + 20792.54079n_a^2,$$
$$1.33 \le n_a \le 1.43, \quad ARS = 0.99633, \tag{2}$$
$$\lambda_h(\text{nm}) = 9294.55n_a - 12498.42,$$
$$1.44 \le n_a \le 1.54, \quad ARS = 0.99886, \tag{3}$$

where λ_l and λ_h are the resonant wavelengths of the two RI subranges of analyte, and n_a is the RI of the analyte.

Table 1. Performance comparison among various SPR-based fiber sensors.

Fiber structure	Detection RI range/RIU	Sensitivity/(nm/RIU)	*ARS*	Ref.
Selectively coated HF	1.33–1.41	2728 (average)	0.85365	[9]
SMF with titled grating	1.4211–1.4499	454 (average)	–	[19]
Multimode fiber with probe-coated S_iO film	1.4344–1.5859	1023.24 (average)	0.8624	[20]
Analyte filled HF, $d_c = 0.8$*pitch	1.33–1.42	4200 (max)	0.97351	[10]
HF with a side core	1.33–1.43	5000 (max)	0.99633	This work
	1.44–1.54	9294.55 (average)	0.99886	

Table 1 shows the performances of the liquid RI fiber sensors based on SPR mechanism. It is clear that our SCHF-SPR sensor has a larger detection RI range. The sensitivity of the SCHF-SPR sensor is comparable to those of other fiber sensors at lower RI values. But for higher RI, the sensitivity and linearity of our SCHF-SPR sensor are extremely high. The sensing performance of the SCHF-SPR sensor can be improved by adding an air hole in the right silicon core, or adjusting the SCHF structure parameters such as the radius of the first ring of the air hole, the radius of the analyte channel, etc. The structural optimization is believed to enlarge the field overlap between core mode and SPP mode, therefore the sensitivity of the sensor is improved.

5. Conclusions

In this paper we have proposed an SCHF-SPR sensor with a side core directly exciting the plasmon mode of the analyte channel. It reduces the gold consumption and facilitates analyte filling. With a polarizer, the excitation of the guided mode can be realized easily. The calibration relation shows that the maximum sensitivity in an RI range of 1.33 to 1.44 reaches 5000 nm/RIU, and the average sensitivity in an RI range of 1.44 to 1.54 is 9295 nm/RIU, with a high ARS.

References

[1] Lee B, Roh S and Park J 2009 *Opt. Fiber Technol.* **15** 209
[2] Yang P F, Gu Y and Gong Q H 2008 *Chin. Phys. B* **17** 3880
[3] Du Y, Li S G and Liu S 2012 *Chin. Phys. B* **21** 094219
[4] Qin W, Li S G, Xue J R, Xin X J and Zhang L 2013 *Chin. Phys. B* **22** 074213
[5] Lin K Q, Wei L M, Zhang D G, Zheng R S, Wang P, Lu Y H and Ming H 2007 *Chin. Phys. Lett.* **24** 3081
[6] Jiri H, Sinclair S Y and Gunter G 1999 *Sensors and Actuators B* **54** 3
[7] Schmidt M A, Sempere L N P, Tyagi H K, Poulton C G and Russell P St J 2008 *Phys. Rev. B* **77** 033417
[8] Hassani A and Skorobogatiy M 2006 *Opt. Express* **14** 11616
[9] Yu X, Zhang Y, Pan S S, Shum P, Yan M, Yehuda Leviatan and Li C M 2010 *J. Opt.* **12** 015005
[10] Zhang Y T, Xia L, Zhou C, Yu X, Liu H R, Liu D M and Zhang Y 2011 *Opt. Commun.* **284** 4161
[11] Zhou C, Zhang Y T, Xia L and Liu D M 2012 *Opt. Commun.* **285** 2466
[12] Saitoh K, Sato Y and Koshiba M 2003 *Opt. Express* **11** 3188
[13] Russell P St J 2006 *J. Lightwave Technol.* **24** 4729
[14] Brechet F, Marcou J, Pagnoux D and Roy P 2000 *Opt. Fiber Technol.* **6** 181
[15] Zhang Y T, Zhou C, Xia L, Yu X and Liu D M 2011 *Opt. Express* **19** 22863
[16] Yu X, Zhang S, Zhang Y, Ho H P, Shum P, Liu H and Liu D 2010 *Opt. Express* **18** 17950
[17] Shuai B B, Xia L, Zhang Y T and Liu D M 2012 *Opt. Express* **20** 5974
[18] Zhang Z H, Shi Y F, Bian B M and Lu J 2008 *Opt. Express* **16** 1915
[19] Shevchenko Y Y and Albert J 2007 *Opt. Lett.* **32** 211
[20] Zeng J and Liang D 2006 *J. Intell. Mater. Syst. Struct.* **17** 787